Proteome Dynamics During Transition From Exponential to Stationary Phase Under Aerobic and Anaerobic Conditions in Yeast

Authors

Maxime den Ridder, Wiebeke van den Brandeler, Meryem Altiner, Pascale Daran-Lapujade, and Martin Pabst

Correspondence

p.a.s.daran-lapujade@tudelft.nl;
m.pabst@tudelft.nl

In Brief

S. cerevisiae is a widely studied eukaryotic model organism and cell factory. Despite decades of research, its metabolic regulation is still not fully understood. Therefore, we conducted a proteome dynamics study that covers the transition from exponential to stationary phase for both aerobically and anaerobically grown yeast. This study is an important step towards better understanding the impact of glucose exhaustion and oxygen on proteome allocation, and it provides a resource for the development of resource allocation models.

Graphical Abstract
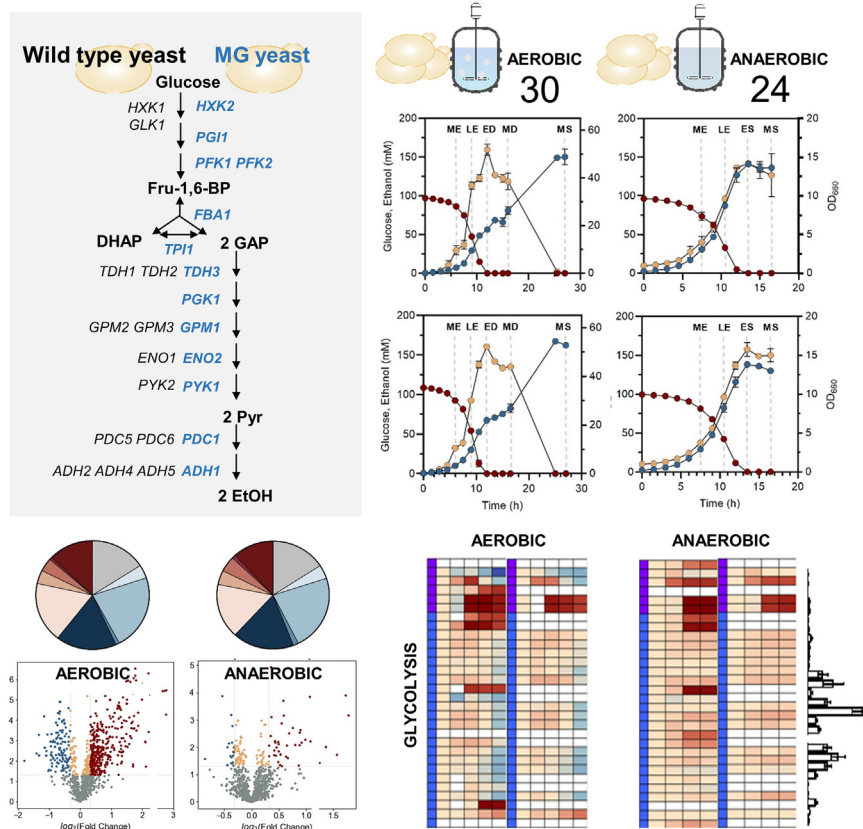
Highlights

- Yeast study covering 54 proteomes during nutrient exhaustion under various conditions.
- Highly controlled reactor experiments with WT yeast and a minimal glycolysis strain.
- Anaerobic cultures show remarkably fewer proteome changes during nutrient exhaustion.
- Proteome dynamics resource for proteome allocation models and metabolic engineering.

Proteome Dynamics During Transition From Exponential to Stationary Phase Under Aerobic and Anaerobic Conditions in Yeast

Maxime den Ridder, Wiebeke van den Brandeler⬤ , Meryem Altiner,
Pascale Daran-Lapujade* ⬤ , and Martin Pabst* ⬤

The yeast *Saccharomyces cerevisiae* is a widely-used eukaryotic model organism and a promising cell factory for industry. However, despite decades of research, the regulation of its metabolism is not yet fully understood, and its complexity represents a major challenge for engineering and optimizing biosynthetic routes. Recent studies have demonstrated the potential of resource and proteomic allocation data in enhancing models for metabolic processes. However, comprehensive and accurate proteome dynamics data that can be used for such approaches are still very limited. Therefore, we performed a quantitative proteome dynamics study to comprehensively cover the transition from exponential to stationary phase for both aerobically and anaerobically grown yeast cells. The combination of highly controlled reactor experiments, biological replicates, and standardized sample preparation procedures ensured reproducibility and accuracy. In addition, we selected the CEN.PK lineage for our experiments because of its relevance for both fundamental and applied research. Together with the prototrophic standard haploid strain CEN.PK113-7D, we also investigated an engineered strain with genetic minimization of the glycolytic pathway, resulting in the quantitative assessment of 54 proteomes. The anaerobic cultures showed remarkably less proteome-level changes compared with the aerobic cultures, during transition from the exponential to the stationary phase as a consequence of the lack of the diauxic shift in the absence of oxygen. These results support the notion that anaerobically growing cells lack resources to adequately adapt to starvation. This proteome dynamics study constitutes an important step toward better understanding of the impact of glucose exhaustion and oxygen on the complex proteome allocation process in yeast. Finally, the established proteome dynamics data provide a valuable resource for the development of resource allocation models as well as for metabolic engineering efforts.

The yeast *Saccharomyces cerevisiae* is a widely-used eukaryotic model organism and cell factory that represents a promising alternative to the fossil fuel–based production of chemicals. However, economic competitiveness is still a major hurdle for such cell factories. Constructing improved strains that realize high productivity and yield involves extensive genetic engineering to rewire native genomes that have been optimized for growth and survival over millions of years of evolution. Nevertheless, intensive research over the past decades have led to successful developments where yeast processes were brought to an industrial scale, such as for the production of the drug precursor artemisinic acid (1–4). *In silico* approaches to reproduce and predict microbial metabolism have been simultaneously developed to assist metabolic engineering efforts (5). However, the complexity of yeast metabolism limits the predictive power of these models. A promising approach to improve such models is to consider resource allocation and more particularly the cost of protein expression (6–10). A prerequisite for this approach is the availability of comprehensive and accurate proteome dynamics data established under tightly controlled conditions. Unfortunately, such data are commonly not available and are difficult to obtain.

S. cerevisiae displays a remarkable metabolic flexibility, as it tunes its metabolism between full respiratory sugar dissimilation and alcoholic fermentation, with different degrees of respirofermentative metabolism as a function of environmental cues, substrate, and oxygen supply. The well-known Crabtree effect results in partial repression of respiration and therefore in respirofermentative growth in the presence of excess sugar (*e.g.*, glucose or galactose) even in aerobic conditions (11). Conversely, the production of gluconeogenic substrates as ethanol or acetate leads to strict respiratory metabolism in aerobic settings. *S. cerevisiae* will fully ferment carbon sources in the absence of oxygen. However, respiratory and

---

fermentative substrate dissimilation have a large impact on ATP yield, as full respiration of 1 mol of glucose results in 16 mol of ATP, whereas fermentation of the same amount of glucose only yields 2 mol of ATP (12). The metabolic mode therefore strongly affects cellular resources, in particular their optimum allocation for growth and survival. To obtain a better insight into how *S. cerevisiae* responds to changes in substrate and oxygen supplies, we monitored its proteome employing tightly controlled bioreactors. Several yeast proteomics studies have already been performed over the past decades (13–21). In this study, however, we monitored the dynamic proteome responses to substrate availability during all growth phases of yeast (exponential, diauxic, and stationary phases) under both aerobic and anaerobic conditions (22). Thus far, only little has been known regarding the proteome dynamics under anaerobic conditions, in particular during transition from the exponential phase to the stationary phase. Studies on changes in the yeast proteome during this transition under anaerobic conditions are currently limited to two-dimensional gel electrophoresis approaches (23–25).

Considering eukaryotes, such as *S. cerevisiae*, genetic redundancy is another level of complexity for *in silico* design and experimental development of cell factories. Many genes, more particularly those involved in metabolism, have orthologs with similar functions (26), but often with a poorly understood physiological role. In view of minimal genomes, several studies have explored the requirement for these redundant genes and implemented top–down approaches to reduce genetic redundancy (27–29). Such minimized genomes have the potential to facilitate the complete redesign and construction of entirely synthetic yeast genomes. Moreover, genetic minimization of key metabolic pathways can facilitate the formulation and validation of mathematical models by eliminating isoenzymes with different regulatory and kinetic properties. Solis-Escalante *et al.* (29)constructed a yeast strain in which the 26 genes encoding enzymes of the Embden–Meyerhof–Parnas pathway of glycolysis, the main pathway for sugar utilization, were minimalized to a set of 13 genes in the minimal glycolysis (MG) strain (Fig. 1*A*). While this genetically reduced strain appeared physiologically comparable to its parent strain (with the full set of glycolytic genes), the underlying proteome dynamics and potential protein level adjustments were not investigated. In this study, the engineered MG strain IMX372 and its parental *S. cerevisiae* CEN.PK113-7D were investigated together during transition from the exponential phase to the stationary phase in the presence or the absence of oxygen. The temporal proteome dynamics across all growth phases were monitored from triplicate bioreactor cultures. Quantitative shotgun proteomic experiments were performed using 10-plex tandem mass tag (TMT) isobaric labeling. The use of tightly controlled reactor experiments in combination with robust sample preparation protocols allows the establishment of highly accurate quantitative data, which constitute valuable resources for *in silico* approaches,

including metabolic engineering effort assistance. Furthermore, the established proteome dynamics data expand the current understanding of protein dynamics in yeast during carbon-limited growth under both aerobic and anaerobic conditions from the proliferation to the stationary phase. Finally, the comparison to the MG mutant quantified the impact of the loss of the minor glycolytic isoenzymes on the global proteome.

EXPERIMENTAL PROCEDURES

Yeast Strains and Media

The MG yeast strain IMX372 (*MATa ura3-52 his3-1 leu2-3112 MAL2-8c SUC2 glk1::SpHis5, hxk1::KlLEU2, tdh1::KlURA3, tdh2, gpm2, gpm3, eno1, pyk2, pdc5, pdc6, adh2, adh5, adh4*) and CEN.PK113-7D (*MATa MAL2-8C SUC2*) used in this study share the CEN.PK genetic background (29, 30). Shake flask and batch cultures were grown in synthetic medium (SM) containing 5.0 g/l (NH₄)SO₄, 3.0 g/l KH₂PO₄, 0.5 g/l MgSO₄·7H₂O, and 1 ml/l trace elements in demineralized water, set at pH 6. The medium was heat sterilized (120 °C) and supplemented with 1 ml/l filter-sterilized vitamin solution and 20 g/l heat-sterilized (110 °C) glucose (self-monitored glucose) (31). The bioreactor medium was supplemented with 0.2 g/l antifoam Emulsion C (Sigma) or with 0.2 g/l antifoam Pluronic PE 6100 (BASF) for anaerobic and aerobic cultures, respectively. In case of anaerobic cultivations, the medium was also supplied with anaerobic growth factors, 10 mg/l ergosterol (Sigma–Aldrich), and 420 mg/l Tween-80 (polyethylene glycol sorbate monooleate; Merck) dissolved in ethanol. Frozen stocks of *S. cerevisiae* cultures were prepared by the addition of glycerol (30% v/v) in 1 ml aliquots for storage at –80 °C.

Bioreactor Cultures

Aerobic shake flask cultures were grown at 30 °C in an Innova incubator shaker (New Brunswick Scientific) at 200 rpm using 500 ml round-bottom shake flasks containing 100 ml medium. Triplicate aerobic batch cultures of control and MG yeast were performed in 2 l laboratory fermenters (Applikon) with a 1.2 l working volume under aerobic and anaerobic conditions. SM was used and maintained at pH 5 by the automatic addition of 2 M KOH. Mixing of the medium was performed with stirring at 800 rpm. Gas inflow was filter sterilized, and compressed air (Linde Gas) or nitrogen (<10 ppm oxygen; Linde Gas) was sparged *via* the bottom of the bioreactor at a rate of 500 ml/min, for aerobic and anaerobic cultures, respectively. Dissolved oxygen levels were measured with Clark electrodes (Mettler Toledo). The temperature of the fermenters was maintained at 30 °C. The reactors were inoculated with exponentially growing shake flask cultures of *S. cerevisiae* strain IMX372 and CEN.PK113-7D to obtain an initial absorbance at 660 nm of approximately 0.2. Sampling for HPLC and absorbance at 600 measurements was done every 90 min. Proteome samples were taken at 6, 9, 12, 16.5, and 27 and at 7.5, 10.5, 13.5, and 16.5 h in aerobic and anaerobic conditions, respectively.

Biomass, Metabolites, and Gas Measurements

To monitor growth, absorbance at 660 nm measurements was performed on a JENWAY 7200 spectrophotometer (Cole-Parmer). The biomass dry weight was determined in duplicate as described earlier (31). For extracellular metabolite determinations, broth samples were centrifuged for 5 min at 13,000*g*, and the supernatant was collected for analysis by HPLC using an Aminex HPX-87H ion exchange column (Agilent). The HPLC was operated at 60 °C, and 5 mM of H₂SO₄ was used as mobile phase at a rate of 0.6 ml/min. Off-gas concentrations

of CO_2 and O_2 were measured using an NGA 2000 analyzer. Proteome samples (~3–5 mg dry weight) were taken from batch cultures. The samples were collected in multifold in trichloroacetic acid (TCA) (Merck Sigma; catalog no.: T0699) with a final concentration of 10%. Samples were centrifuged at 4000g for 5 min at 4 °C. Cell pellets were frozen at −80 °C (32)

Yeast Cell Lysis, Protein Extraction, and Proteolytic Digestion

Cell pellets of the aerobic and anaerobic cultures were resuspended in lysis buffer composed of 100 mM triethylammonium bicarbonate containing 1% SDS and phosphatase/protease inhibitors. Yeast cells were lysed by glass bead milling by 10 cycles of 1 min shaking alternated with 1 min rest on ice. Proteins were reduced by addition of 5 mM DTT and incubation for 1 h at 37 °C. Subsequently, the proteins were alkylated for 60 min at room temperature in the dark by addition of 50 mM acrylamide. Protein precipitation was performed by addition of four volumes of ice-cold acetone (−20 °C), followed by 1 h freezing at −20 °C. The proteins were solubilized using 100 mM ammonium bicarbonate. Proteolytic digestion was performed by Trypsin (Promega), 1:100 enzyme to protein ratio, and incubated at 37 °C overnight. Solid phase extraction was performed with an Oasis HLB 96-well µElution plate (Waters) to desalt the mixture. Eluates were dried using a SpeedVac vacuum concentrator at 50 °C and frozen at −80 °C.

Quantitative Temporal Proteome Analysis

Desalted peptides were reconstituted in 100 mM triethylammonium bicarbonate, and TMT10-plex reagents (Thermo) were added from stocks dissolved in 100% anhydrous acetonitrile (ACN). Peptides were mixed with labels in a 1:8 ratio (12.5 µg to 100 µg) and incubated for 1 h at 25 °C and 400 rpm, and the labeling reaction was stopped by addition of 5% hydroxylamine to a final concentration of 0.4%. Labeled peptides were then mixed in approximately equal quantities. Two bridging samples were included in each TMT10-plex experiment to improve comparability between different experiments. The bridging sample was a mixture of the three biological replicates of MG yeast under aerobic conditions in the midstationary (MS) phase. Peptide solutions were diluted with water to obtain a final concentration of ACN lower than 5%. Solid phase extraction was performed to desalt the final peptide mixture. Desalted peptides were subsequently frozen at −80 °C for 1 h and dried by vacuum centrifugation. Peptides were finally resuspended in 3% ACN/0.01% TFA prior to MS analysis to give an approximate concentration of 500 ng per µl. Samples were labeled as indicated in supplemental Table S3.

Shotgun Proteomic Analysis

An aliquot corresponding to approximately 1 µg protein digest was analyzed using a one-dimensional shotgun proteomics approach (33). Briefly, the samples were analyzed using a nano–liquid chromatography system consisting of an EASY nano-LC 1200, equipped with an Acclaim PepMap RSLC RP C18 separation column (50 µm × 150 mm, 2 µm; catalog no.: 164568), and a QE plus Orbitrap mass spectrometer (Thermo Fisher Scientific). The flow rate was maintained at 350 nl/min over a linear gradient from 5% to 25% solvent B over 180 min, then from 25% to 55% over 60 min, followed by back equilibration to starting conditions. Data were acquired from 5 to 240 min. Solvent A was H_2O containing 0.1% formic acid, and solvent B consisted of 80% ACN in H_2O and 0.1% formic acid. The Orbitrap was operated in data-dependent acquisition mode acquiring peptide signals from 385 to 1250 m/z at 70 K resolution in full mass spectrometric mode with a maximum ion injection time of 75 ms and an automatic gain control target of 3E6. The top ten precursors were selected for MS/MS analysis and subjected to fragmentation using higher-energy collisional dissociation. MS/MS scans were acquired at 35 K resolution

with automatic gain control target of 1E5 and injection time of 100 ms, 1.2 m/z isolation width, and normalized collision energy of 32.

Processing of Mass Spectrometric Raw Data

Data were analyzed against the proteome database from *S. cerevisiae* (UniProt, strain ATCC 204508/S288C, Tax ID: 559292, July 2020) using PEAKS Studio X (version 10.0) (Bioinformatics Solutions, Inc) (34), allowing for 20 ppm parent ion and 0.02 m/z fragment ion mass error, three missed cleavages, acrylamide, and TMT10 label as fixed and methionine oxidation and N/Q deamidation as variable modifications. Peptide spectrum matches (PSMs) were filtered against 1% false discovery rates (FDRs), and the protein identifications required ≥2 unique peptides. For analysis of labeling completeness, the mass of the TMT10plex label was set as variable modification for lysine and N-terminal residues. The labeling efficiency was expressed as percent of labeling of available lysine and N-terminal residues (supplemental Table S3). In addition, overlabeling was estimated by database searching of spectra that were not identified in the first round searches in which the TMT label was set as fixed modification for lysine and N-terminal residues. For this, the TMT label was set as variable modification for lysine and N-terminal residues as well as for serine, threonine, and tyrosine residues, or alternatively, the TMT label was set as variable modification without any restrictions. Quantitative analysis was performed on protein identifications containing at least two unique peptides, which peptide identifications were filtered against 1% PSM FDR (see supplemental Table S3 for obtained PSM, peptide, and protein FDR values per experiment). TMT reporter ion intensities of the individual experiments were extracted using the TMT quantification option provided by the PEAKSQ software tool (Bioinformatics Solutions, Inc). PEAKSQ settings were set to autonormalization without applying reporter ion and minimum quality thresholds. PEAKSQ reports were exported to "proteins.csv" files containing the quantified proteins.

Experimental Design and Statistical Rationale

Briefly, the exported "proteins.csv" files from PEAKSQ, listing the quantified proteins for each experiment (supplemental Table S14), were imported into the Python environment. Normalization between data was performed using a bridging sample. A function was further established that links UniProt accession numbers and yeast genes (as obtained from https://www.uniprot.org/docs/yeast.txt) and which subsequently was used to annotate identified proteins from the experiments with correct gene names. The biological triplicates per condition (aerobic and anaerobic) and strain (control and MG) were treated separately for creating the clustermaps (see later). Furthermore, each biological replicate consisted of two additional averaged technical replicates. To analyze the reproducibility of the experiments, clustermaps were made using the clustermap function from the Seaborn package in Python (35), using the Euclidean distances metric and the average linkage method. Only proteins detected in all three biological replicates were used for the cluster analysis. The fold change of each protein in a specific condition was calculated relative to the bridging sample. Finally, averages of the three biological replicates per condition were determined to obtain the four subdatasets (i) control aerobic, (ii) MG aerobic, (iii) MG anaerobic, and (iv) control anaerobic. All graphs ultimately show the analyses of these biological-replicate averages and their corresponding standard deviations. The statistical significance of changes between individual time points or growth conditions was determined using a two-sided t test (also known as Welch's t test) using the ttest_ind_from_stats function from the "SciPy.stats" module in Python. Experimental variations are expressed as relative standard deviation (%) between the obtained values of the normalized biological replicates. Estimation of required number of replicates for different experimental variations (5, 10, 15, 20,
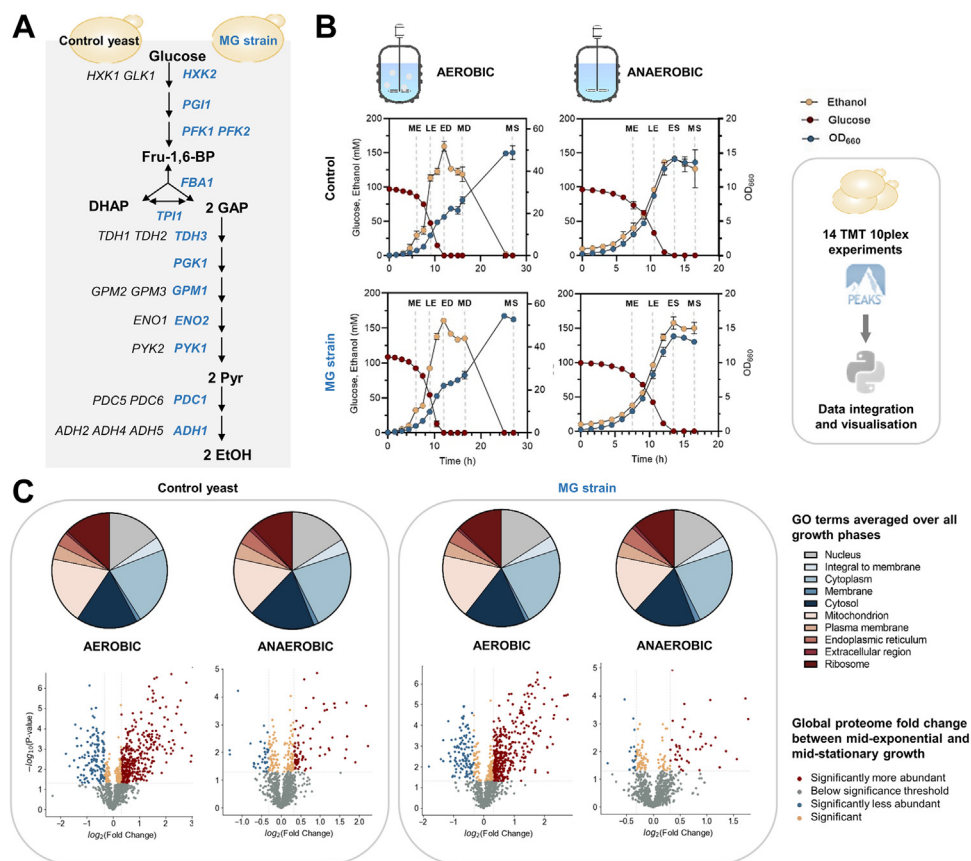
Fig. 1. Yeast proteome dynamics study capturing the transition from proliferation to stationary phase under aerobic and anaerobic conditions. *A*, schematic overview of glycolysis in the yeast control strain (CEN.PK113-7D, *black*) and the minimal glycolysis (MG) strain (IMX372, *blue*). The enzymes in *blue* are retained in MG yeast. *B*, yeast growth in aerobic and anaerobic cultures. Glucose (*red*) and ethanol (*yellow*) concentrations and absorbance at 660 nm (*blue*, secondary *y*-axis) were measured during the different growth phases of aerobic and anaerobic batch cultures for the control yeast and the MG strain. The values shown are averages obtained from three biological replicates. Standard deviations are indicated by error bars. The *dotted gray lines* indicate time points at which samples were taken for proteome analysis. Proteome samples were taken from each biological replicate in the aerobic cultures after 6, 9, 12, 16.5, and 27 h of growth, in the midexponential (ME), late-exponential (LE), early diauxic (ED), mid-diauxic (MD), and midstationary (MS) growth phase, respectively. Furthermore, proteome samples were taken off the anaerobic cultures after 7.5, 10.5, 13.5, and 16.5 h of growth, in the ME, LE, early stationary (ES), and MS growth phase, respectively. Proteome samples were subjected to quantitative shotgun proteomics experiments, using 10-plex tandem mass tag (TMT) isobaric labeling and a one-dimensional, 4-h chromatographic separation. Database searching and quantitative analysis were performed using PEAKS X and using a tailor-made Python data processing pipeline. *C*, annotation of yeast protein functions using Gene Ontology (GO) terms. Based on the classifications of GO annotation, the overall functions of the identified yeast proteins (with at least two unique peptides present) were categorized into cellular component and displayed in pie chart format with absolute protein numbers (average of three biological replicates). The global proteome changes between the ME and MS phase under aerobic and anaerobic conditions in control and MG strain were visualized using volcano plots. The fold changes were normalized to the aerobic and anaerobic ME phases. The log2 of the abundance fold change between the two conditions was plotted against the significance (–log10p), using a *p* value threshold of <0.05 and a fold change threshold of >1.25 (which corresponds to a log2 fold change threshold of ±0.32). Significant changes of MS proteins were colored by their direction of change (*red* if higher, *blue* if lower, or *peach* if similar to their ME equivalents). The total number of proteins with changes are listed in Table 1.

and 30% relative standard deviation) and fold change levels (1.25-, 1.5-, 2-, 2.5-, and 3-fold) were performed using the python "statsmodels module," obtained from https://www.statsmodels.org, stats.power.TTestIndPower. Solve_power(), using alpha = 0.05 and a power of 0.8 (supplemental Table S2 and supplemental Fig. S4) (36).

The power calculations for individual fold changes between time points or growth conditions were performed using the python "statsmodels module" (see aforementioned) using the calculated *p* value (alpha) of the respective fold change or a fixed *p* value (alpha) of 0.05 (supplemental Fig. S5; supplemental Tables S8, S9 and S11–S13) (36).

Pathway Analysis, Functional Enrichment, and Data Visualization

To study how protein abundances changed in individual cellular pathways, the obtained proteomics data were analyzed using the KEGG (Kyoto Encyclopedia of Genes and Genome) pathway database (37). All the up-to-date KEGG pathways were retrieved with the constructed "KEGG_tool.py" code. Here, the Bio.KEGG.REST module from the Biopython package in Python was used (38). Thereby, the function "kegg_list" was used to list all pathways for *S. cerevisiae* and "kegg_get" to retrieve gene names that are assigned to a specific pathway. The central carbon metabolism (CCM) pathways were

reduced to the most important genes in order to enable meaningful visualization in graphs. Using the aforementioned clustermap function, the protein fold changes of the CCM were plotted on a heat map for each of the experiments, without any clustering. For better visualization of the trends, the data were normalized to the midexponential (ME) phase. The same function was moreover used to display the average absolute intensity of every protein throughout the whole growth curve, using log10 and absolute scale, respectively. The significance of a difference in biological-replicate-average fold changes between two datasets was assessed by performing a two-sided two-sample unpaired t test (also known as Welch's t test), using the "ttest_ind_from_stats" function from the "SciPy.stats" module in Python (39). Global proteome changes between two experiments or phases were visualized in volcano plots, where the $-10\log10(p)$ is plotted against the $\log2$(fold change) between the two conditions. These plots were generated using the "gene_exp.volcano," a modified version of the GeneExpression.volcano function from the "Bioinfokit.visuz" module in Python (https://github.com/reneshbedre/bioinfokit). This function enabled the division of the fold changes between two experiments into (*i*) insignificant changes, (*ii*) statistically significant changes (but not necessarily biologically significant), and (*iii*) statistically and likely biologically significant changes. For this study, the statistical significance threshold was generally set to $p < 0.05$. The (presumed) biological significance threshold was set to a log2 fold change threshold of ±0.32 (indicating a 1.25 absolute fold change).

A functional enrichment analysis using the STRING database was performed in order to determine whether specific Gene Ontology (GO) terms or KEGG pathways are enriched under a particular condition (40). For this, Python was used to programmatically access the STRING database *via* an application programming interface. This created a dictionary containing the upregulated and downregulated proteins, the species identifier (4932 for *S. cerevisiae*), the functional categories that should be assessed, the FDR threshold (<0.05 in this study), and an optional set of "background genes" with an alternative background as the whole species proteome. The function "backgroundgene_2_string" retrieves the protein-specific string identifiers for the background genes/proteins, which in this case were all proteins detected across the experiments.

Estimation of the average protein content for the aerobic and anaerobic growth conditions using emPAI and PAI indices was performed according to Yasushi Ishihama *et al.* (41). Circle graphs were made using the "surf" function in Matlab, where circle areas represent the obtained emPAI values. UpSet plots (42) to identify and visualize unique and shared proteins and peptides per experiment were created using Matlab (123695-upset-plot, version 1.1.0, matlabcentral/fileexchange, Zhaoxu Liu, 2023).

RESULTS

Proteome Dynamics of Laboratory Control CEN.PK113-7D and MG Yeast in Aerobic and Anaerobic Batch Bioreactor Cultures

To optimize data reproducibility and reliability, we performed the batch cultures in bioreactors in which mixing, aeration, and pH were tightly controlled. Independent triplicate cultures were conducted for the two investigated strains to further increase biological significance. Furthermore, we selected the prototrophic control strain *S. cerevisiae* CEN.PK113-7D—a popular lineage for biotechnology for which several omics datasets are already available—and the MG variant (IMX372) lacking glycolytic minor isoenzymes, for

our study (Fig. 1*A*). The batch cultures were sampled during all growth phases, ranging from the proliferation phase to growth arrest in the stationary phase (Fig. 1*B*). Generally, the presence or the absence of oxygen is known to strongly affect yeast physiology, which results in differences in metabolism and growth phases. During growth on glucose, aerobic cultures both respire and ferment, producing ethanol and other fermentation products. The growth on glucose is followed by a diauxic growth phase during which fermentation products are fully respired until the stationary phase. Conversely, *S. cerevisiae* fully ferments glucose and does not respire in the absence of oxygen. Dissimilation of fermentation products requires oxygen; therefore, anaerobic cultures directly switch from exponential growth on glucose to the stationary phase, without a diauxic phase. These physiological differences were also observed in the growth and metabolite profiles performed in our study (supplemental Table S1 and Fig. 1*B*). Aerobic proteome dynamics were monitored in time with sampling at 6, 9, 12, 16.5, and 27 h of growth, corresponding to the ME, late exponential, early diauxic, mid-diauxic, and stationary growth phases, respectively (Fig. 1*B*). To align the sampling time points to the physiology, we sampled the anaerobic cultures at 7.5, 10.5, 13.5, and 16.5 h of growth, corresponding to the ME and late exponential, early stationary, and stationary growth phases, respectively (Fig. 1*B*). After cell lysis and trypsin digestion, peptide samples of three biological replicates per condition were labeled using TMT10-plex reagents, mixed equally, and subjected to a 4 h (gradient) shotgun proteomics experiment (supplemental Table S3). On average, 1175 and 1106 proteins were quantified in the control yeast under aerobic and anaerobic conditions, respectively, with at least two unique peptides and 1% FDR. Similarly, 1131 and 1127 proteins were quantified confidently on average for the aerobic and anaerobic cultures of the MG strain, respectively. In total, 1734 different proteins were quantified of which 1069 proteins were shared between all conditions (supplemental Fig. S1 and supplemental Tables S4 and S5). The protein amount was estimated using the emPAI index (41), and the total protein content was estimated by summing all emPAI values, thereby assuming for unidentified proteins the lowest observed emPAI value of our study. This indicated that more than 99% of the protein mass was captured in our study (supplemental Fig. S2 and supplemental Table S6). The detected proteins were predominantly assigned to intracellular organelle functional GO categories, consisting of cytosolic, mitochondrial, and ribosomal proteins (Fig. 1*C* and supplemental Table S7), which could be explained by their high expression levels (19, 43). A similar GO term assignment was found for both strains and conditions.

The crude protein quantification profiles were further analyzed using a Python data processing pipeline to enable a tailored visualization and interpretation of the large-scale data. To this end, the data from the 14 separate TMT experiments (supplemental Table S3) were compared for their temporal and

conditional protein abundance changes in the control strain (CEN.PK113-7D) and MG yeast strain IMX372 under (an)aerobic conditions. Data were presented as fold changes for each protein in a specific condition relative to a bridging sample. The bridging (control) sample used in all TMT experiments was a mixture of the three biological replicates of the aerobic stationary phase MG yeast to improve comparability between the experiments (supplemental Table S3). The labeling efficiency for each TMT experiment was >95% (supplemental Table S3), whereas overlabeling was assessed and exemplified for one TMT experiment and resulted in <5% of the PSMs containing excess TMT labels.

To assess experimental reproducibility, we compared global proteomic data with cluster analysis data based on Euclidean distances using three biological replicates per strain and condition and two technical replicates per time point within each biological replicate. This demonstrated clustering of replicates of the different growth phases per strain and condition, confirming the reproducibility of the reactor experiments and proteomic analyses (supplemental Fig. S3). Furthermore, the overall experimental variation was very low, whereas the statistical power was generally high, and at least three numbers of biological replicates for the obtained experimental variations were calculated to be required (supplemental Table S2, supplemental Figs. S4 and S5). Because of the extended chromatographic separation, significant interference from cofragmentation for the employed moderate isolation window (1.2 m/z) was likely low. Nevertheless, this maintained sensitivity and ultimately provided a very reproducible analysis. However, further improvements could be expected by employing a mass spectrometric 3-based quantification strategy. The average protein abundance of the three biological replicates per condition was used for the interpretation of the proteome dynamics data.

Effects of Oxygen Availability on the Global Proteome Dynamics Across the Growth Curve

To explore the impact of oxygen availability on the yeast proteome, we first focused on the growth phases with the most marked change in the global proteome between the aerobic and anaerobic cultures for the control strain CEN.PK113-7D (*i.e.*, stationary and ME phases). While a similar number of proteins were quantified in the presence and absence of oxygen, the number of differently expressed proteins between the stationary and ME phases varied significantly between both conditions (p value of < 0.05 and fold change of ±1.25). For the aerobic cultures, 364 proteins were significantly more abundant under carbon starvation (stationary phase), whereas this only accounted for 78 proteins under anaerobiosis (Fig. 1*C* and Table 1). A significantly lower abundance was also observed in the stationary phase for 174 proteins than in the exponential growth phase in the presence of oxygen and for 42 proteins only in the absence of oxygen (Fig. 1*C* and Table 1).

Deprived of usable carbon source, stationary-phase yeast cells generally arrest growth, thereby entering a state of decreased metabolism and biosynthesis and yielding overall lower transcription and translation rates (44, 45). Ribosomal proteins have been shown to be expressed at lower levels in the stationary phase (46, 47). In good agreement with physiological data, the proteins involved in processes associated with protein synthesis and cellular growth showed decreased abundance in the transition between the exponential and stationary growth phases under both aerobic and anaerobic conditions, as shown in the categories "gene expression," "ribosome assembly," and "cellular macromolecule biosynthetic process" (supplemental Tables S8 and S9). Yeast cells transition from respirofermentation on glucose to full respiration using ethanol as a primary carbon source in the presence of oxygen. This increase in respiratory activity was well reflected in the proteome in this study, as proteins more abundant in the stationary phase were typically associated with mitochondrial respiration in the aerobic conditions, including "generation of precursor metabolites and energy," "mitochondrion organization," and "transmembrane transport" (supplemental Table S8). As expected, this response was not observed in the nonrespiring anaerobic cultures. In these cultures, most proteins involved in carbohydrate catabolic and disaccharide metabolic processes showed an increased abundance in the stationary compared with the ME phase, presumably to ensure survival in growth-arrested cells. Proteins in the cellular components involving categories such as "cell periphery" and "plasma membrane" were also found to be more abundant (supplemental Table S9).

The comparison of the proteomic data across the growth phases revealed that the diauxic shift had the strongest impact on proteomic rearrangement, with 24 proteins with lower abundance and 125 proteins with higher abundance between the beginning of the diauxic growth and mid-diauxic phases (Table 1 and supplemental Table S8). The diauxic shift was characterized by an increased abundance in proteins involved in aerobic respiration, fatty acid metabolism, and precursor metabolite and energy generation, in line with the switch from respirofermentative to fully respiratory metabolism. Conversely, the set of proteins with decreased abundance during the diauxic shift was enriched for proteins involved in protein synthesis in the cytosol. This result was also consistent with the decreased growth rate and thereby the protein synthesis rate of yeast cells grown on ethanol media as compared with glucose (48). Under anaerobiosis, most proteomic changes occurred in the transition between exponential and stationary growth (55 proteins; *i.e.*, 46% of all detected changes in abundance throughout the phases). Notably, prolonged cultivation during the stationary phase under anaerobiosis did not further alter the proteome (Table 1 and supplemental Table S9).

Impact of Oxygen on the Proteomic Rearrangements in the CCM Across the Growth Phases

The CCM consists of key pathways required for the conversion of carbon sources into the 12 building blocks for the synthesis of cellular components and encompasses ca. 150 transport proteins and enzymes (28). The flow of carbon and electrons *via* the CCM therefore responds to the carbon source nature and abundance. As oxygen availability dictates how much ATP molecules can be produced from the carbon source, the CCM also responds to oxygen availability. The proteins involved in the CCM are therefore expected to be considerably affected by glucose and oxygen availability. In our study, 101 of 142 CCM proteins (supplemental Table S10) were successfully quantified in at least one of the main four conditions (Fig. 2*A*). In the presence of oxygen, 71 proteins had significantly different abundance over the time course, whereas in the absence of oxygen, only 18 significant changes were observed.

S. cerevisiae harbors a set of 17 proteins able to transport hexoses, known as Hxt proteins. The expression of these proteins is primarily dictated by hexose (mostly glucose) abundance. Being membrane bound and having low abundance, Hxt proteins are typically difficult to detect in proteomic studies; their high level of homology makes their identification challenging. Nevertheless, six Hxt proteins were quantified in the present dataset: Hxt2, 3, 4, 5, 6, and 7. Four of these Hxt proteins could be quantified in all samples, irrespective of strain and oxygen supply. Hxt6 and Hxt7 share a high protein sequence similarity (>99%) and were therefore considered as one protein group in this study. These were the most abundant Hxt proteins and were consistently more abundant upon glucose exhaustion in all tested conditions (Fig. 2*A*), in good agreement with their high affinity for glucose (49). The abundance of Hxt4, a high-affinity transporter, expectedly increased upon glucose exhaustion but decreased upon reaching the stationary phase in the aerobic cultures; meanwhile, it remained high under anaerobiosis. The low-affinity transporter Hxt3 was detected at high and low glucose concentrations (50) but decreased in abundance across the growth curve and most significantly in the aerobic stationary phase as has been observed in stationary phase yeast before (15). Hxt5 was only detected in the control strain in the presence of oxygen, but its abundance was in line with its induction by nonfermentable carbon sources and decreasing growth rates (49). Hxt2 was only detected in the anaerobic cultures of the control strain. Thereby, Hxt2 increased in abundance upon glucose exhaustion, as expected for a high-affinity transporter.

Among the 26 glycolytic and fermentation enzymes, 13 major isoforms are constitutively expressed with high abundance, whereas the remaining are minor isoforms with lower abundance and condition-dependent expression (29, 51). This notion was well reflected in the present comprehensive

TABLE 1
Number of proteins with significant changes during the transition to subsequent growth phase under aerobic and anaerobic conditions for the yeast control strain (CEN.PK113-7D)

CEN.PK113-7D growth transition	# Proteins quantified	# More abundant	# Less abundant
Anaerobic			
Late exponential/ME	1092	1	22
Early stationary/late exponential	1092	52	3
Stationary/early stationary	1092	0	0
Stationary/ME	1092	78	42
Aerobic			
Late exponential/ME	998	12	21
Early diauxic/late exponential	998	67	4
Mid-diauxic/early diauxic	1168	125	24
Stationary/mid-diauxic	1168	90	34
Stationary/ME	1168	364	174

The total number of proteins indicates the number of proteins that were detected in at least two biological replicates. Proteins were normalized to the preceding growth phase. Only proteins with a fold change of 1.25 or greater (which corresponds to a log2 fold change of ±0.32) and a *p* value of at least 0.05 are considered. The number of proteins quantified indicates the number of proteins that were detected and quantified in at least two biological replicates.

dataset, in which 23 of these proteins could be quantified in both conditions of the control strain. All major isoenzymes were found; their abundance remained constant under anaerobiosis but slightly decreased in the stationary phase under aerobiosis (Fig. 2*A*). The majority of the minor isoenzymes were detected in at least one of the conditions. The minor glyceraldehyde-3P dehydrogenase Tdh1 was found to be expressed with and without oxygen. However, the enzyme was generally more abundant upon glucose exhaustion. Similarly, Glk1 and Hxk1, glucose-repressed isoenzymes of the predominant hexokinase 2, were also more abundant upon glucose exhaustion. Adh2, alcohol dehydrogenase repressed by glucose and induced by ethanol (52), was only detected in the presence of oxygen, and its abundance strongly increased in the mid-diauxic phase. Interestingly, the estimated total amount of the glycolytic enzymes was larger than the sum of the other CCM enzymes in all conditions (Fig. 2, *B* and *C*).

The TCA cycle, encompassing a set of 22 proteins located in the mitochondrion, is particularly active during respiration. The majority of the TCA cycle proteins were detected in our experiments. Their abundance generally strongly increased during the diauxic shift but did not change under anaerobic conditions (Fig. 2*A*). A small group of proteins remained unaffected during progression through the growth phase under anaerobiosis. For example, Pda1, Pdb1, and Lat1, which are three of the five subunits of the pyruvate dehydrogenase complex, Aco2 and Idp1 remained unchanged. Interestingly, Frd1 and Osm1, which are important for protein folding in anaerobic conditions (53), also remained unaffected. Many

CCM metabolites cross the mitochondrial membrane *via* transporter proteins, and increased respiratory activity, are expected to increase the flux of metabolites between the cytosol and mitochondria. Accordingly, the abundance of the seven quantified mitochondrial transporters increased after glucose exhaustion aerobically but not anaerobically, with a marked increase for Odc1 and Sfc1, which are carboxylic acid antiporters. Despite the increase in respiratory activity during the diauxic shift and phase, which was reflected in the TCA cycle proteins, the abundance of anaplerotic proteins, Pyc1, Pyc2, and Mae1, remained unchanged. Conversely, the abundance of the gluconeogenic proteins Fbp1 and Pck1 and glyoxylate cycle proteins MLs1 and Icl1 required for ethanol utilization strongly increased upon glucose exhaustion aerobically but was expectedly very stable anaerobically. Growth on nonfermentable carbon sources requires a complex metabolic rearrangement to supply cytosolic and mitochondrial acetyl-CoA. The expression of the proteins involved in acetate and acetyl-CoA metabolism, particularly Acs1 and Ach1, accordingly increased during the diauxic phase but was not visibly affected by glucose exhaustion under anaerobiosis.

Redox metabolism, a key for cell survival, is balanced according to oxygen availability. While respiring cells can oxidize the NADH produced during glucose assimilation *via* oxidative phosphorylation, two-step glycerol formation from dihydroxyacetone phosphate is the major electron sink in the absence of oxygen. The abundances of paralogs Gpd1, Gpd2, Gpp1, and Gpp2 were not strongly affected across the different phases and growth conditions (supplemental Fig. S6*A*), which is in agreement with the reported transcriptional regulation and (in)activation by post-translational modification (phosphorylation) (54). The only noticeable changes were the decreased abundance of Gpp1 in the presence of oxygen and increased abundance of Gpp2 upon glucose exhaustion in the absence of oxygen. In aerobic conditions, NADH is generally oxidized by external or internal NADH dehydrogenases, which shuttle the electrons into the mitochondrial electron transfer chain. Contrarily, anaerobic yeast cultures reoxidize the excess NADH formed during biosynthesis *via* glycerol production (55). The increased abundance of Gut2 during the diauxic shift under aerobiosis can be explained by both its role in glycerol utilization and redox balance maintenance (supplemental Fig. S6*A*).

Oxygen-Dependent Dynamics in Other Pathways

Respiration is an important mechanism for energy conservation in the presence of the electron acceptor oxygen. After the diauxic shift, respiration becomes the main ATP source for the cells. Accordingly, the abundance of the ATP synthases and cytochrome oxidases in the oxidative phosphorylation pathway increased significantly after glucose exhaustion (supplemental Fig. S9). However, the abundance of these proteins remained constant over the entire growth curve in the

anaerobic cultures. Respiring cells are prone to generation of reactive oxygen species, for instance by the production of superoxide during electron transfer during oxidative phosphorylation, which can induce the expression of stress tolerance genes (56). Accordingly, Sod1 and Sod2, enzymes that detoxify superoxide and produce hydrogen peroxide (57) were significantly more abundant under the aerobic conditions than under the anaerobic conditions (supplemental Fig. S9). Their abundance increased by at least twofold toward the stationary phase compared with that under log growth in the presence of oxygen, whereas the protein abundance remained constant under anaerobic growth. A similar protein profile was found for the peroxisomal and mitochondrial catalase A (Cta1) that detoxifies hydrogen peroxide. Nevertheless, the abundance of Ccs1, copper ion chaperone to Sod1, was relatively constant and similar between both conditions in the control strain (supplemental Fig. S9).

Heme synthesis, encompassing a set of eight Hem proteins, also depends on oxygen availability (58). In this study, seven Hem proteins could be quantified. The protein abundance of Hem2, 3, 12, and 15 was either similar between the aerobic and anaerobic conditions or higher aerobically (Fig. 3*A*). However, Hem1, Hem13, and Hem14 were only quantified or higher abundant under anaerobic conditions, although Hem14 could be quantified only in one biological replicate based on a few peptides. Hem13 was confidently quantified with more than ten peptides for each biological anaerobic replicate but was not found aerobically. Surprisingly, both Hem13 and Hem14 require oxygen for enzymatic activity.

Finally, sterol synthesis also requires oxygen, and ergosterol is therefore supplied as an anaerobic growth factor during anaerobic yeast cultures (59, 60). Herein, 17 Erg proteins were found in either the aerobic condition or the anaerobic condition or both (Fig. 3*B*). The Erg proteins that need oxygen, such as Erg1, Erg3, Erg11, and Erg25 to 28, were either solely present anaerobically or more abundant in the anaerobic cultures than in the aerobic cultures.

Survival in the Stationary Phase in Response to Oxygen Availability

A previous study has shown a strong effect of oxygen availability and the presence of transition through the diauxic phase on yeast cell robustness during the stationary phase (61). This work proposed that oxygen availability had a positive effect on the adenylate energy charge, longevity, stress response, and thermotolerance during the stationary phase. However, this study was based on changes in the transcript levels, without confirmation at the protein level. In particular, limited data are known regarding the proteome dynamics under anaerobic conditions. To fill this knowledge gap, we studied the proteomic differences between the stationary phase in the anaerobic and aerobic conditions. A total of 249 proteins were significantly more abundant, and 125 were less abundant in the presence of oxygen than in the absence of
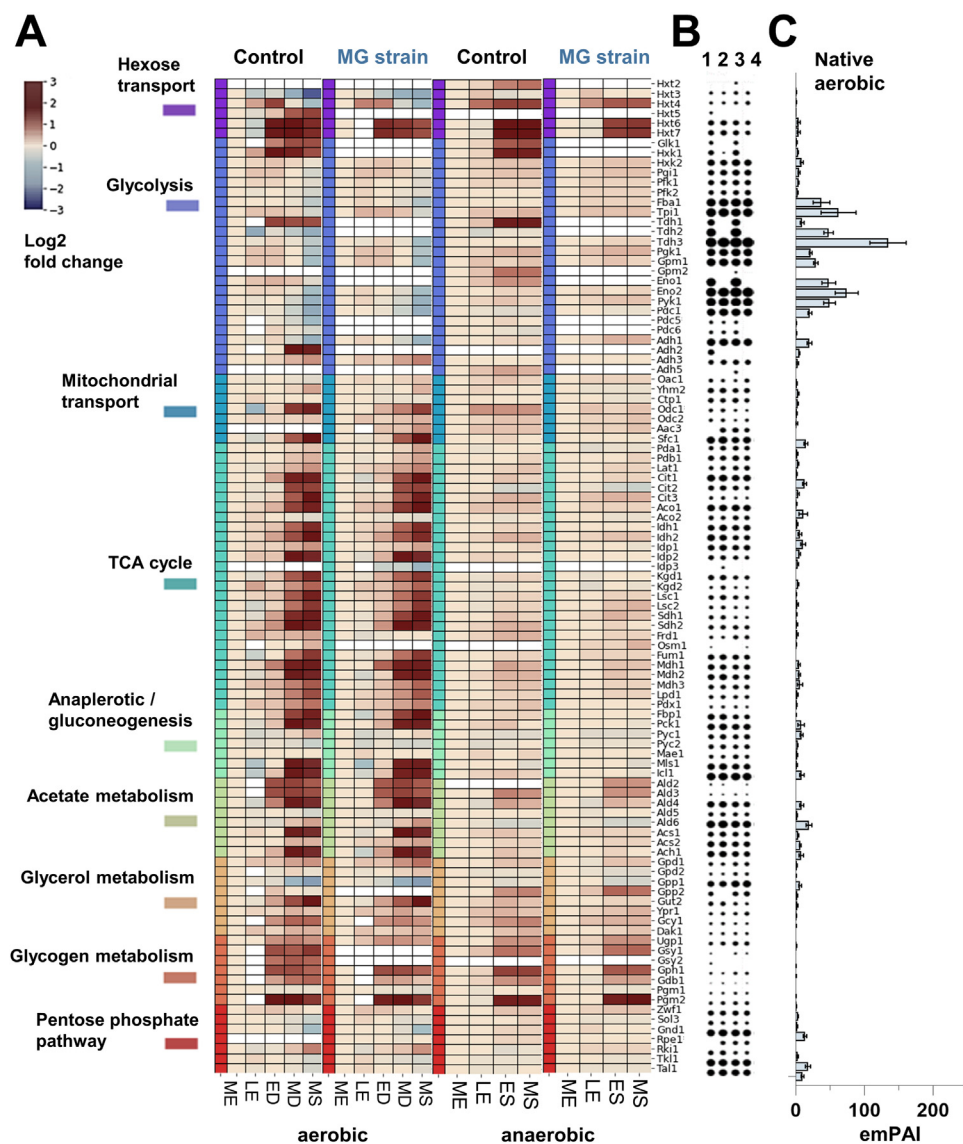
FIG. 2. **Yeast central carbon metabolism protein abundances under aerobic and anaerobic growth.** *A*, the heat map shows the temporal log2 fold changes of the enzymes of the central carbon metabolism (CCM) of the control yeast CEN.PK113-7D and minimal glycolysis (MG) yeast for the midexponential (ME), late-exponential (LE), early diauxic (ED), mid-diauxic (MD), early stationary (ES), and midstationary (MS) phases, compared with the ME phase for each condition. The proteins belonging to specific pathways of the CCM are highlighted with different colors. *White gaps* in the map indicate that the protein was not detected or that it has been deleted in case of the MG strain. No filtering for significance or fold-change thresholds was applied for this figure, and all enzymes that were detected were included in the heat map. *B* and *C*, the circle graph (1 = control aerobic, 2 = MG aerobic, 3 = control anaerobic, and 4 = MG anaerobic) on the *right* express the emPAI values of the individual proteins for each condition as *circle* areas. The bar graph on the *right* shows the averaged emPAI values per enzyme. Standard deviations are indicated by the error bars in the bar graph.

oxygen (*p* value of < 0.05 and fold change of ±1.25; supplemental Table S11 and supplemental Fig. S7). In the stationary phase, the aerobic cells still relied on respiration, and the proteins involved in respiration were accordingly more abundant under the aerobic conditions. Conversely, the yeast cells entered the stationary phase rather abruptly after glucose depletion under the anaerobic conditions. The proteins associated with "biosynthesis," "glycolysis," and "cytoplasmic translation" were more abundant in the anaerobic stationary

cells than in the aerobic cells, as well as several ribosomal proteins. Furthermore, the proteins involved in storage metabolism, in particular glycogen metabolism, were enriched anaerobically.

Yeast cells generally accumulate storage carbohydrates in sugar-rich conditions that can be used as carbon and energy source to ensure survival during the stationary phase. Anaerobic cultures are entirely dependent on glycogen and trehalose as energy storage components. Conversely, the
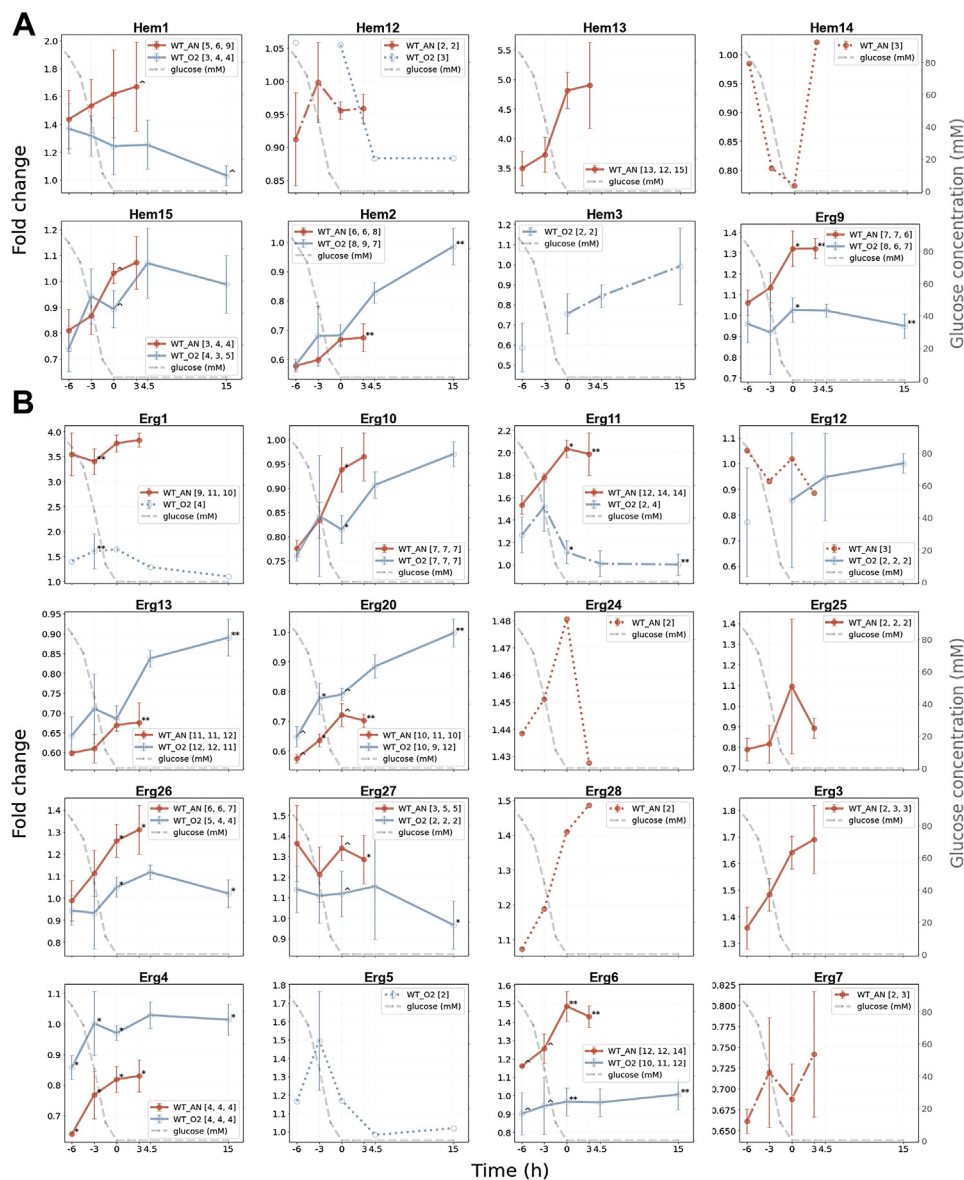
FIG. 3. **Protein fold-change line graphs for nonrespiratory oxygen-dependent pathways during aerobic and anaerobic growth.** The fold-change values were plotted against the time relative to glucose depletion ($t = 0$) in hours for proteins involved in heme (*A*) and sterol (*B*) synthesis. The different colors of the line graphs represent "*orange*" the control yeast strain under anaerobic conditions (WT_AN) and "*light blue*" the control strain under aerobic conditions (WT_O2). The line graphs represent the average of the three biological replicates, where the error bars indicate the standard deviation. The *gray dashed line* represents the glucose concentration over time (mM, secondary *y*-axis). The number of quantified peptides per biological replicate are shown in *brackets*. *Asterisks* (*) and *circumflexes* (ˆ) indicate the significance (*p* values) between the aerobic and anaerobic experiments as follows: $p < 0.001$ (***), $p < 0.01$ (**), $p < 0.05$ (*), and $p < 0.1$ (ˆ).

presence of oxygen enables yeast cells to metabolize other available nutrients, such as lipids and amino acids (62–64). In this study, profiles of proteins involved in glycogen metabolism showed similar trends, as the protein abundances increased considerably after glucose exhaustion under both aerobic and anaerobic conditions (supplemental Fig. S6*B*). Nevertheless, several proteins involved in glycogen metabolism were more abundant in the anaerobic cultures than in the aerobic cultures, including enzymes involved in glycogen

generation, Pgm2 and Ugp1. Other proteins toward glycogen synthesis (such as Pgm1, Glg1, Glg2, and Glc3) were not confidently or not at all quantified in our study. Glycogen is finally generated by Gsy1/2, where only Gsy1 was detected in our experiments with sufficient confidence in the anaerobic cultures. Glycogen can also be utilized by Gph1 to form glucose-1P again or by Gdb1 for conversion to glucose. Herein, only Gph1 showed a profile comparable to that of Pgm2, which was also observed previously when assessing

the yeast proteome under different carbon sources. Here, alternative functions in synthesis and breakdown of glycogen were suggested for Pgm1 and Pgm2, respectively (16).

Trehalose is another storage metabolite in yeast, which is synthesized from UDP-glucose. It is converted into trehalose-6P by Tps1 and subsequently into trehalose by Tps2. Trehalose is utilized by Nth1, Nth2, and Ath1 and converted into glucose again. In our study, the enzymes leading up to trehalose had similar protein profiles under the aerobic and anaerobic conditions, and the protein abundance increased significantly after glucose depletion (supplemental Fig. S6B). However, utilization of trehalose was more difficult to capture, as only Nth1 was quantified with only a few unique peptides under the aerobic and anaerobic conditions. Furthermore, in the absence of oxygen, yeast cells could not catabolize fatty acid by beta-oxidation as energy reserve during carbon starvation. Proteins such as Fox2, Pox1, Cat2, and Crc1 showed relatively constant expression levels over the anaerobic growth curve, whereas their abundance increased drastically after glucose depletion in the presence of oxygen (supplemental Fig. S9).

Finally, aerobic stationary-phase cells are known to acquire increased robustness and stress tolerance during transition to the stationary phase. However, previous studies have indicated that this does not apply to anaerobic cultures to the same extent (61). Stress proteins include a range of heat shock proteins (Hsps) with various functions. The fold changes and levels of Hsp were comparable in the presence and absence of oxygen in the exponential growth phase (supplemental Fig. S8), but Hsp was more abundant in both aerobic and anaerobic conditions toward the end of the growth curve in the MS phase. This increase was markedly greater in the aerobically cultured cells, resulting in a significantly lower anaerobic fold change of the proteins in the stationary phase.

Proteome-Level Alterations Following Genetic Minimization of the Glycolytic Pathway

The genetic reduction in the MG strain consisted of the removal of the 13 minor enzymes involved in glycolysis and fermentation, only leaving the 13 major isoenzymes. The present dataset showed that most minor isoenzymes were expressed and quantifiable in all samples from the aerobic and anaerobic batch cultivations, with the exception of Gpm2 and Adh5 detected only in the anaerobic cultures, Adh2 detected only in the aerobic cultures, and Adh4, Gpm3, and Pyk2 not detected at all (Fig. 4). Tdh2, Eno1, and Adh2 were abundant in the batch cultures, and deletion of the minor isoenzymes might therefore affect the yeast physiology. The MG strain was previously well characterized by physiological and transcriptome analyses in the presence of oxygen, revealing that the physiology and transcriptome of this strain was nearly identical to that of the control strain with a full set of glycolytic and fermentation genes (29). However, the proteome of the

MG strain was not explored, and limited data are known regarding the response of the MG strain to anaerobiosis. The fluxes through glycolysis and the fermentation pathway are substantially higher in anaerobiosis than in aerobiosis (65), and the deletion of all minor isoenzymes might therefore have a different cellular impact in the presence and absence of oxygen. As previously observed, the physiology of the MG and control strains in the aerobic and anaerobic cultures was nearly identical (supplemental Table S1) (29).

The difference in the abundance of the glycolytic and fermentation proteins between the MG and parental control strains was assessed by comparing the expression levels across the entire growth curve using a two-sided two-sample t test. Remarkably, all major isoenzymes displayed identical time profiles between the MG and control strains; they were very stable under anaerobiosis, but their profiles decreased after the mid-diauxic phase under aerobiosis (Fig. 4). With the exception of Fba1 and Tdh3, the abundance of the glycolytic and fermentation proteins was well conserved between the MG and control strains. The abundance of Tdh3 was consistently higher across all growth phases by 40 to 50% in the MG strain compared with the control strain anaerobically (p value of < 0.01). The estimated protein amount of Tdh2 in the control strain was approximately one-third of the estimated protein amount of Tdh3 both under the aerobic and anaerobic conditions (Fig. 5). The Tdh1 levels also markedly increased after glucose depletion in the control strain (Fig. 2A). The loss of these relatively abundant minor isoenzymes and subsequent overall reduction of glyceraldehyde-3P activity in the MG strain might have caused a crossregulation and an increased abundance of Tdh3. Interestingly, while the minor isoenzyme Eno1 was also abundant in the control strain (Fig. 5), its deletion had no visible effect on the Eno2 level in the MG strain (Fig. 4). The abundance of Fba1 was slightly (approximately 20–40%) but significantly higher in the MG strain than in the control strain both in the presence and absence of oxygen. Fba1 does not have isoenzymes, and this difference in abundance could therefore not be attributed to crossregulation. Fba1 is an abundant protein in yeast, operating far from saturation (65); the flux through glycolysis did not increase in the MG strain compared with that in the control strain. This increase in the abundance of Fba1 is therefore not likely explained by the need for a higher aldolase capacity in the MG strain.

The enzyme level adjustments within the glycolytic and fermentation pathways following the deletion of the minor isoenzymes were remarkably small but slightly more pronounced under the anaerobic conditions. In line with this subtle phenotype, the proteome was not visibly affected by the deletion of the minor isoenzymes (cutoff p value of 0.05 [5%], fold change threshold of ±1.25; Table 2 and supplemental Tables S12 and S13). Consequently, no enriched or depleted GO terms or KEGG pathways could be identified. The metabolic comparability between both strains
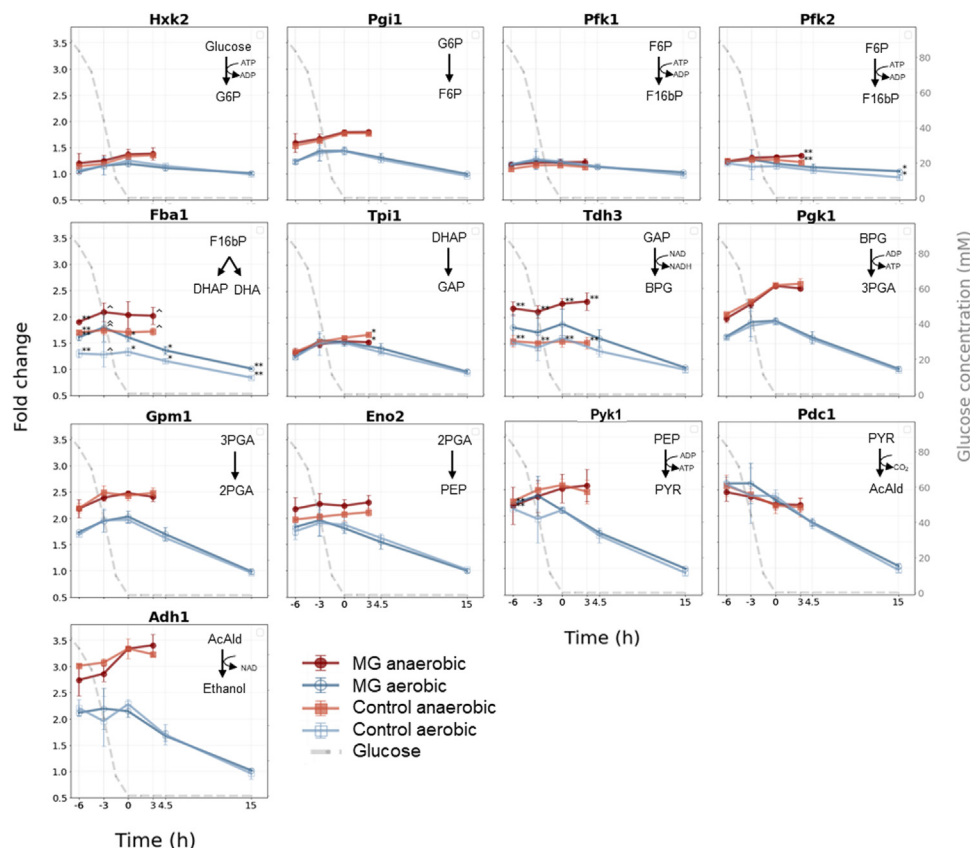
FIG. 4. **Protein fold-change line graphs for the major glycolytic enzymes under aerobic and anaerobic growth.** The fold-change values were plotted against the time relative to glucose depletion ($t = 0$) in hours for all proteins of the major glycolytic enzymes. The different colors of the line graphs represent "*red*" for the minimal glycolysis (MG) strain under anaerobic conditions, "*dark blue*" the MG strain under aerobic conditions, "*orange*" for the control yeast strain under anaerobic conditions, and "*light blue*" for the control strain under aerobic conditions. Shown are the average values of the biological triplicates where the error bars indicate the standard deviations. The *gray dashed line* represents the glucose concentration over time (mM, secondary *y*-axis). *Asterisks* (*) and *circumflexes* () indicate the significant changes between the control and MG strain. *p* Values are indicated as follows: <0.001 (***), <0.01 (**), <0.05 (*), and <0.1 ().

is therefore underlined by their similar CCM enzyme (Fig. 2*A*) and global proteome profiles.

DISCUSSION

To the best of our knowledge, this study provides the most comprehensive proteomic study on the response of *S. cerevisiae* CEN.PK113-7D to both oxygen and nutrient availability. We employed tightly controlled batch bioreactor cultures and performed biological triplicates combined with standardized sample preparation protocols to ensure high reproducibility and accuracy. Albeit different yeast proteome dynamics studies have been performed over the past decades (16, 18, 20, 66), no study has yet captured the complete spectrum of conditions using the same strain and the same highly controlled experimental setup. Moreover, the transition from the exponential to the stationary phase under anaerobic conditions has not yet been investigated. This study moreover quantified the impact of genetic minimization of the glycolytic pathway on proteome resource allocation using the recently

established MG strain (23). The established dataset therefore covers the quantitative analysis of 54 individual proteomes, where approximately 99% of the expressed protein mass (based on emPAI calculations, supplemental Fig. S2) have been captured. The high reproducibility was also highlighted by the strong similarities between the proteomes of the MG and control strains. This comprehensive and accurate dataset therefore provides an ideal resource for applied and fundamental studies in yeast and more particularly for *in silico* proteome allocation studies.

The most remarkable observation was the substantially smaller proteome response of yeast cells grown under anaerobiosis than under aerobiosis. In both conditions, yeast cells had to tune their metabolism to the transition from glucose excess to exhaustion, leading to a shift from exponential to stationary growth. However, these drastic changes triggered a far milder response than did the aerobic transition to and out of the diauxic phase, which represented 58% of the measured changes in protein abundance. During the diauxic shift, cells rewire the proteome for respiratory growth on

ethanol as a main carbon source. This transition leads to a multitude of physiological and morphological changes, including smaller cell size, increased mitochondrial volume, decreased growth rate, increased respiration rate, and therefore increased ROS production, induction of gluconeogenesis and the glyoxylate cycle, and large changes in the fluxes in CCM. These changes were well reflected by the observed changes in the proteome allocation in this study. For instance, an increase in mitochondrial protein abundance was observed, whereas the glycolytic proteins were simultaneously downregulated under aerobic conditions (13–15, 67).

Using the exact same strain and experimental setup, Bisschops *et al.* (61) showed a stronger and faster decrease in viability upon glucose exhaustion for anaerobic cultures than for aerobic cultures. Based on physiological and transcriptome data, the authors attributed this lack of robustness to the inability of cells to adapt to glucose exhaustion in the absence of oxygen. Conversely, the diauxic shift provides the resources needed to transition from fast growth to growth arrest in the presence of oxygen. Furthermore, yeast cells obtained through long-term cultivation with total cell retention under calorie restriction acquired a higher stress tolerance and better adaptation to starvation in comparison to cells grown in carbon-rich environments under both aerobic and anaerobic conditions (68, 69). However, in these studies, yeast cells obtained a higher robustness in the presence than in the absence of oxygen. The present proteomics study supports this view in different ways. The small protein response during transition from sugar excess to depletion suggests that the anaerobic cells do not have the means or proper regulatory network to adjust to the new conditions. Furthermore, aerobic cultures acquire robustness and stress tolerance during transition to the stationary phase as a result of the expression of the "stress-response" genes (70), such as Hsp. Both aerobic and anaerobic cultures showed a similar "stress signaling" as shown by the increase in the Hsp level toward the stationary phase; however, this increase was far less pronounced in the anaerobic cultures. The abundance of Hsp was therefore substantially lower in the absence of oxygen, in line with the lower transcription of Hsp and lower thermotolerance of the anaerobic stationary-phase cultures than of the aerobic cultures observed by Bisschops *et al.* (61). Considering that industrial-scale processes favor anaerobic environments for practical and financial reasons, the present results provide valuable information for the construction of predictive metabolic models (5, 9, 71–76).

In the presence of oxygen, yeast cells switch from respirofermentative to full respiratory metabolism once glucose is depleted. Accordingly, the abundance of respiration-related proteins increased upon glucose exhaustion in the aerobic cultures herein, whereas their protein profiles remained constant in the anaerobic cultures, which was in agreement with previous yeast proteome studies (15, 20). Several other nonrespiratory pathways in *S. cerevisiae*, such as fatty acid beta-oxidation and heme and sterol synthesis, are oxygen dependent. Expectedly, most detected proteins in these pathways were aerobically more abundant or contained similar abundance profiles to the anaerobic cultures. Nevertheless, oxygen-dependent protein Hem13 involved in heme synthesis was only confidently quantified under anaerobic conditions, and the lack of detection in the aerobic conditions suggests that Hem13 is far less abundant. The transcription of Hem1*3* is repressed by oxygen and heme itself (77, 78); therefore, this protein lacks repression in the absence of oxygen, and its abundance is thereby increased. Similar protein profiles under anaerobic conditions were previously found for Hem1, Hem14, and Hem15 (18). Several oxygen-dependent Erg proteins were also more abundant or solely detected under anaerobiosis. Herein, the transcription of various Erg proteins was regulated by oxygen, and an absence increased the expression of these Erg proteins (79, 80). Nevertheless, it should be taken into account that under aerobic conditions, ergosterol is synthesized in the cell, whereas in the absence of oxygen, it is exogenously supplied.

Glycolysis and alcoholic fermentation are well-studied pathways that play an important role in sugar conversion in the industry. The present proteome dataset showed that the abundance of most major glycolytic isoenzymes decreased during the diauxic shift and further decreased during the stationary phase in the presence of oxygen. Conversely, their abundance was unaffected during transition to the stationary phase under the anaerobic environments. Aerobic cultures in the stationary phase therefore display substantially lower glycolytic enzyme levels than do anaerobic cultures. For instance, a 2.5- to 3.5-fold lower abundance was observed for Pgk1, Gpm1, Pdc1, and Adh1. While this difference in abundance is not expected to affect survival in the stationary phase, in which the glycolytic flux is extremely low or absent, it will influence the ability of stationary-phase cells to reach fast growth when transitioned to a sugar-rich medium. When exposed to anaerobic sugar excess, cells grown aerobically to the stationary phase have to allocate resources to increase the abundance of glycolytic enzymes and reach fast growth, whereas cells precultured anaerobically do not. As glycolytic enzymes are, next to ribosomal proteins, the most abundant proteins, this aspect should be considered during the start-up phase of anaerobic industrial fermentations and their modeling.

The expression of the minor glycolytic isoenzymes is condition dependent, and several of these isoenzymes are reported to have distinct functions, especially during changes in carbon source availability. The present dataset showed that the presence of oxygen only visibly affected the abundance of Eno1, Tdh1, and Hxk1, as their abundance was significantly higher after glucose depletion under anaerobic conditions than under aerobic conditions (Fig. 2). While some minor
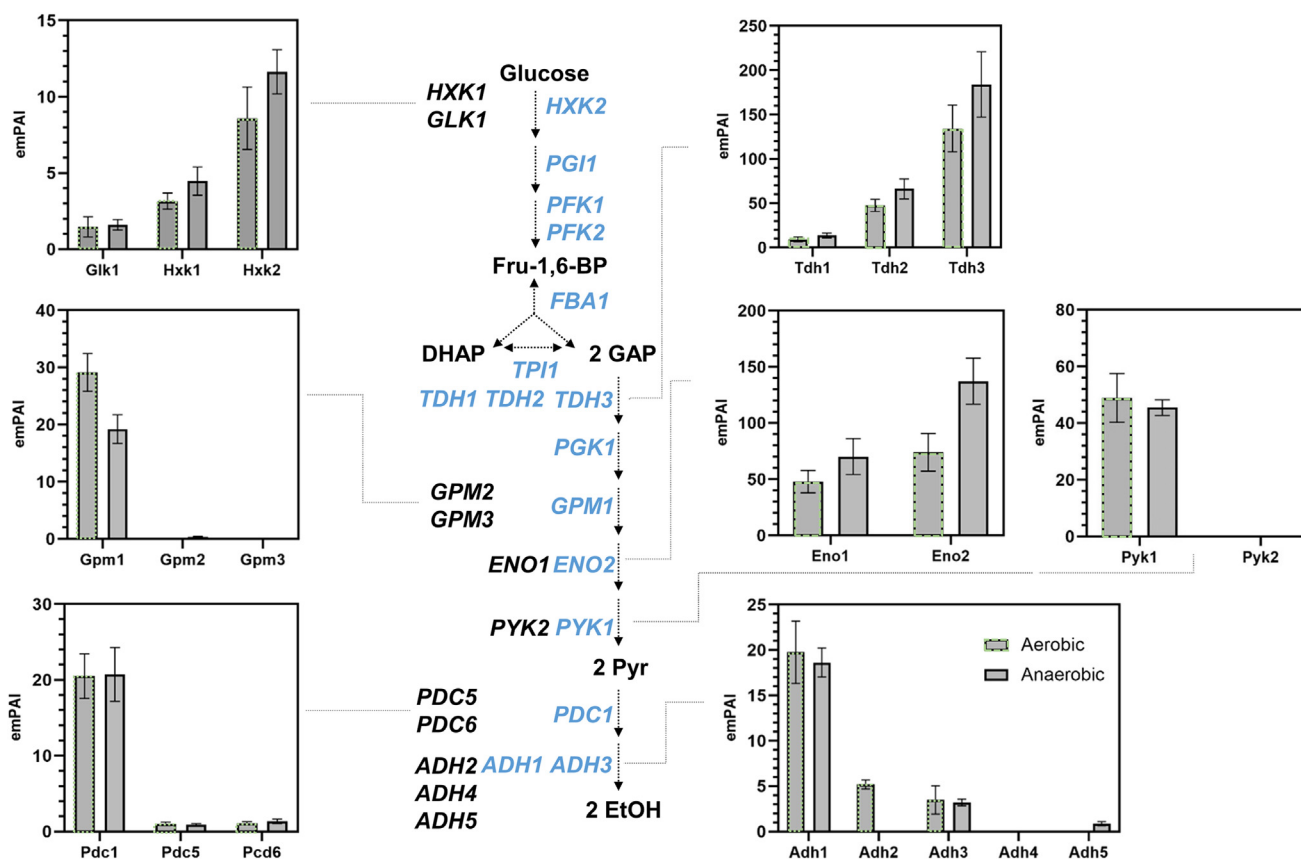
FIG. 5. **Abundance bar graphs for the glycolytic isoenzymes under aerobic and anaerobic conditions for the yeast control strain (CEN.PK113-7D).** The bar graphs show the averaged protein abundances for the observed glycolytic isoenzymes expressed by their emPAI (exponentially modified protein abundance) indices, under aerobic (*gray bars* with *green dashed lines*) and anaerobic (*gray bars*) growth. The bars represent the average values of the individual biological replicates (with at least one identification per replicate), where the error bars indicate the standard deviation.

isoenzymes had a substantial abundance in yeast (Fig. 5), with the exception of Tdh3, their removal did not trigger visible changes in the abundance of the major isoenzymes. Tdh3, glyceraldehyde dehydrogenase major isoenzyme, notably increased by 1.5-fold in the MG strain as compared with the control strain under anaerobic conditions (Fig. 4). The same trend was observed aerobically, albeit much less pronounced. Similar to most glycolytic enzymes, glyceraldehyde dehydrogenase operates at overcapacity, meaning that the enzyme capacity largely exceeds the flux catalyzed *in vivo* (81). Therefore, the increased abundance of Tdh3 in the MG strain does most likely not result from the need to compensate for Tdh1 and Tdh2 deletion to maintain the glycolytic flux. Glyceraldehyde dehydrogenase isoenzymes do not have any well-described moonlighting functions. However, next to their cytosolic localization, they are also found in the cell wall in which they might play a yet uncovered role (82). The composition and structure of *S. cerevisiae* cell wall are affected by oxygen, and several cell wall proteins are specifically enriched under anaerobiosis (*e.g.*, cell wall mannoprotein of the Srp1p/Tip1p family), which might explain the

observed crossregulation in the MG strain. Herein, Fba1 was also mildly but significantly upregulated in the MG mutant both aerobically (1.2–1.4-fold change) and anaerobically (1.15-fold change). As Fba1 does not have isoenzymes and is solely responsible for the glycolytic flux, its change in abundance is difficult to explain. Fba1 is also involved in vacuolar function as a subunit of the vacuolar V-ATPase (83). However, as no or minimal differences were observed in the other components of V-ATPase between the MG and control strains, the molecular mechanism leading to the slightly higher abundance of Fba1 in the MG strain remains unclear. Many factors can alter the functionality of proteins, including post-translational modifications, protein localization, or interactions with other proteins or biomolecules (84, 85). A recent study has suggested that phosphorylation regulates the activity of many glycolytic enzymes (7). However, the stable abundance of glycolytic proteins between the MG and control strains was well reflected in the stability of *in vitro* enzyme activity (29), suggesting the lack of differences in the post-transcriptional regulation between these strains. Taken together, remarkably few proteome-level changes were observed as a consequence of the genetic

TABLE 2

Number of proteins with significant changes between the yeast control strain (CEN.PK113-7D) and MG stain under aerobic and anaerobic conditions

MG mutant *versus* control yeast	# Proteins quantified	# More abundant	# Less abundant
Anaerobic			
ME	978	10	13
Late exponential	978	10	8
Early stationary	978	8	18
Stationary	978	7	6
Aerobic			
ME	1019	18	10
Late exponential	950	33	13
Early diauxic	1019	15	9
Mid-diauxic	1019	3	3
Stationary	1019	3	2

The protein abundances of the MG strain were normalized to the yeast control strain (for the same growth phase and the same condition). Only proteins with a fold change of 1.25 (log2 fold change of ±0.32) or greater and a *p* value of at least 0.05 are considered. The number of proteins quantified indicates the number of proteins that were detected and quantified in at least two biological replicates.

reduction of glycolysis, which is also supported by the lack of response in growth rates and the transcriptome under these standardized conditions (29). This similarity between both strains finally underscores the usefulness of the simplified MG strain for proteome allocation studies and for studying the role of post-translational modifications in the regulation of glycolysis.

The complete proteome dynamics and abundance data for the batch reactor–cultured CEN.PK113-7D strain and the related MG mutant for aerobic and anaerobic growth are shown in supplemental Table S14.

DATA AVAILABILITY

Mass spectrometric raw data have been deposited to the ProteomeXchange Consortium (86) *via* the PRIDE (87) partner repository and are publicly available under the project code PXD031412.

REFERENCES

1. Paddon, C. J., and Keasling, J. D. (2014) Semi-synthetic artemisinin: a model for the use of synthetic biology in pharmaceutical development. *Nat. Rev. Microbiol.* **12**, 355–367
2. Nielsen, J. (2019) Yeast systems biology: model organism and cell factory. *Biotechnol. J.* **14**, 1–9
3. Ro, D. K., Paradise, E. M., Quellet, M., Fisher, K. J., Newman, K. L., Ndungu, J. M., *et al.* (2006) Production of the antimalarial drug precursor artemisinic acid in engineered yeast. *Nature* **440**, 940–943
4. Nielsen, J., Larsson, C., van Maris, A., and Pronk, J. (2013) Metabolic engineering of yeast for production of fuels and chemicals. *Curr. Opin. Biotechnol.* **24**, 398–404
5. Lao-Martil, D., Verhagen, K. J. A., Schmitz, J. P. J., Teusink, B., Wahl, S. A., and van Riel, N. A. W. (2022) Kinetic modeling of Saccharomyces cerevisiae central carbon metabolism: achievements, limitations, and opportunities. *Metabolites* **12**, 74
6. Nilsson, A., and Nielsen, J. (2016) Metabolic trade-offs in yeast are caused by F1F0-ATP synthase. *Sci. Rep.* **6**, 1–11
7. Xia, J., Sánchez, B., Chen, Y., Campbell, K., Kasvandik, S., and Nielsen, J. (2022) Proteome allocations change linearly with specic growth rate of saccharomyces cerevisiae under glucose-limitation. *Nat. Commun.* **13**, 2819
8. Metzl-Raz, E., Kafri, M., Yaakov, G., Soifer, I., Gurvich, Y., and Barkai, N. (2017) Principles of cellular resource allocation revealed by condition-dependent proteome profiling. *Elife* **6**, 1–21
9. Björkeroth, J., Campbell, K., Malina, C., Yu, R., Di Bartolomeo, F., and Nielsen, J. (2020) Proteome reallocation from amino acid biosynthesis to ribosomes enables yeast to grow faster in rich media. *Proc. Natl. Acad. Sci. U. S. A.* **117**, 21804–21812
10. Elsemman, I. E., Rodriguez Prado, A., Grigaitis, P., Garcia Albornoz, M., Harman, V., Holman, S. W., *et al.* (2022) Whole-cell modeling in yeast predicts compartment-specific proteome constraints that drive metabolic strategies. *Nat. Commun.* **13**, 1–12
11. De Deken, R. H. (1966) The crabtree effects and its relation to the petite mutation. *J. Gen. Microbiol.* **44**, 157–165
12. Van Dijken, J. P., Bauer, J., Brambilla, L., Duboc, P., Francois, J. M., Gancedo, C., *et al.* (2000) An interlaboratory comparison of physiological and genetic properties of four Saccharomyces cerevisiae strains. *Enzyme Microb. Technol.* **26**, 706–714
13. Slavov, N., Budnik, B. A., Schwab, D., Airoldi, E. M., and van Oudenaarden, A. (2014) Constant growth rate can be supported by decreasing energy flux and increasing aerobic glycolysis. *Cell Rep.* **7**, 705–714
14. Zampar, G. G., Kümmel, A., Ewald, J., Jol, S., Niebel, B., Picotti, P., *et al.* (2013) Temporal system-level organization of the switch from glycolytic to gluconeogenic operation in yeast. *Mol. Syst. Biol.* **9**, 651
15. Murphy, J. P., Stepanova, E., Everley, R. A., Paulo, J. A., and Gygi, S. P. (2015) Comprehensive temporal protein dynamics during the diauxic shift in *Saccharomyces cerevisiae*. *Mol. Cell. Proteomics* **14**, 2454–2465

16. Costenoble, R., Picotti, P., Reiter, L., Stallmach, R., Heinemann, M., Sauer, U., *et al.* (2011) Comprehensive quantitative analysis of central carbon and amino-acid metabolism in Saccharomyces cerevisiae under multiple conditions by targeted proteomics. *Mol. Syst. Biol.* **7**, 464

17. Picotti, P., Bodenmiller, B., Mueller, L. N., Domon, B., and Aebersold, R. (2009) Full dynamic range proteome analysis of S. cerevisiae by targeted proteomics. *Cell* **138**, 795–806

18. Helbig, A. O., De Groot, M. J. L., Van Gestel, R. A., Mohammed, S., De Hulster, E. A. F., Luttik, M. A. H., *et al.* (2009) A three-way proteomics strategy allows differential analysis of yeast mitochondrial membrane protein complexes under anaerobic and aerobic conditions. *Proteomics* **9**, 4787–4798

19. Ho, B., Baryshnikova, A., and Brown, G. W. (2018) Unification of protein abundance datasets yields a quantitative Saccharomyces cerevisiae proteome. *Cell Syst.* **6**, 192–205.e3

20. de Groot, M. J. L., Daran-Lapujade, P., van Breukelen, B., Knijnenburg, T. A., de Hulster, E. A. F., Reinders, M. J. T., *et al.* (2007) Quantitative proteomics and transcriptomics of anaerobic and aerobic yeast cultures reveals post-transcriptional regulation of key cellular processes. *Microbiology (Reading)* **153**, 3864–3878

21. Di Bartolomeo, F., Malina, C., Campbell, K., Mormino, M., Fuchs, J., Vorontsov, E., *et al.* (2020) Absolute yeast mitochondrial proteome quantification reveals trade-off between biosynthesis and energy generation during diauxic shift. *Proc. Natl. Acad. Sci. U. S. A.* **117**, 7524–7535

22. den Ridder, M., Knibbe, E., van den Brandeler, W., Daran-Lapujade, P., and Pabst, M. (2022) A systematic evaluation of yeast sample preparation protocols for spectral identifications, proteome coverage and post-isolation modifications. *J. Proteomics* **261**, 104576

23. Rossignol, T., Kobi, D., Jacquet-Gutfreund, L., and Blondin, B. (2009) The proteome of a wine yeast strain during fermentation, correlation with the transcriptome. *J. Appl. Microbiol.* **107**, 47–55

24. Noti, O., Vaudano, E., Giuffrida, M. G., Lamberti, C., Cavallarin, L., Garcia-Moruno, E., *et al.* (2018) Enhanced arginine biosynthesis and lower proteolytic profile as indicators of Saccharomyces cerevisiae stress in stationary phase during fermentation of high sugar grape must: a proteomic evidence. *Food Res. Int.* **105**, 1011–1018

25. Trabalzini, L., Paffetti, A., Ferro, E., Scaloni, A., Talamo, F., Millucci, L., *et al.* (2003) Proteomic characterization of a wild-type wine strain of Saccharomyces cerevisiae. *Ital. J. Biochem.* **52**, 145–153

26. Escalera-Fanjul, X., Quezada, H., Riego-Ruiz, L., and González, A. (2019) Whole-genome duplication and yeast's fruitful way of life. *Trends Genet.* **35**, 42–54

27. Luo, Z., Yu, K., Xie, S., Monti, M., Schindler, D., Fang, Y., *et al.* (2021) Compacting a synthetic yeast chromosome arm. *Genome Biol.* **22**, 1–18

28. Postma, E. D., Couwenberg, L. G. F., van Roosmalen, R. N., Geelhoed, J., de Groot, P. A., and Daran-Lapujade, P. (2022) Top-down, knowledge-based genetic reduction of yeast central carbon metabolism. *mBio* **13**, e0297021

29. Solis-Escalante, D., Kuijpers, N. G. A., Barrajon-Simancas, N., van den Broek, M., Pronk, J. T., Daran, J. M., *et al.* (2015) A minimal set of glycolytic genes reveals strong redundancies in saccharomyces cerevisiae central metabolism. *Eukaryot. Cell.* **14**, 804–816

30. Entian, K.-D., and Kötter, P. (2007) 25 yeast genetic strain and plasmid collections. *Methods Microbiol.* **36**, 629–666

31. Verduyn, C., Postma, E., Scheffers, W. A., and Van Dijken, J. P. (1992) Effect of benzoic acid on metabolic fluxes in yeasts: a continuous-culture study on the regulation of respiration and alcoholic fermentation. *Yeast* **8**, 501–517

32. Kanshin, E., Tyers, M., and Thibault, P. (2015) Sample collection method bias effects in quantitative phosphoproteomics. *J. Proteome Res.* **14**, 2998–3004

33. Köcher, T., Pichler, P., Swart, R., and Mechtler, K. (2012) Analysis of protein mixtures from whole-cell extracts by single-run nanolc-ms/ms using ultralong gradients. *Nat. Protoc.* **7**, 882–890

34. Ma, B., Zhang, K., Hendrie, C., Liang, C., Li, M., Doherty-Kirby, A., *et al.* (2003) Peaks: powerful software for peptide de novo sequencing by tandem mass spectrometry. *Rapid Commun. Mass Spectrom.* **17**, 2337–2342

35. Waskom, M. (2021) Seaborn: statistical data visualization. *J. Open Source Softw.* **6**, 3021

36. Levin, Y. (2011) The role of statistical power analysis in quantitative proteomics. *Proteomics* **11**, 2565–2567

37. Kanehisa, M., and Goto, S. (2000) Kegg: kyoto encyclopedia of genes and genomes. *Nucleic Acids Res.* **28**, 27–30

38. Cock, P. J. A., Antao, T., Chang, J. T., Chapman, B. A., Cox, C. J., Dalke, A., *et al.* (2009) Biopython: freely available python tools for computational molecular biology and bioinformatics. *Bioinformatics* **25**, 1422–1423

39. Virtanen, P., Gommers, R., Oliphant, T. E., Haberland, M., Reddy, T., Cournapeau, D., *et al.* (2020) SciPy 1.0: fundamental algorithms for scientific computing in python. *Nat. Methods* **17**, 261–272

40. Jensen, L. J., Kuhn, M., Stark, M., Chaffron, S., Creevey, C., Muller, J., *et al.* (2009) String 8 - a global view on proteins and their functional interactions in 630 organisms. *Nucleic Acids Res.* **37**, 412–416

41. Ishihama, Y., Oda, Y., Tabata, T., Sato, T., Nagasu, T., Rappsilber, J., *et al.* (2005) Exponentially modified protein abundance index (emPAI) for estimation of absolute protein amount in proteomics by the number of sequenced peptides per protein. *Mol. Cell. Proteomics* **4**, 1265–1272

42. Lex, A., Gehlenborg, N., Strobelt, H., Vuillemot, R., and Pfister, H. (2014) UpSet : visualization of intersecting sets. *IEEE Trans. Vis Comput. Graph.* **20**, 1983–1992

43. Kolkman, A., Daran-Lapujade, P., Fullaondo, A., Olsthoorn, M. M. A., Pronk, J. T., Slijper, M., *et al.* (2006) Proteome analysis of yeast response to various nutrient limitations. *Mol. Syst. Biol.* **2**. 2006.0026

44. Fuge, E. K., Braun, E. L., and Werner-Washburne, M. (1994) Protein synthesis in long-term stationary-phase cultures of Saccharomyces cerevisiae. *J. Bacteriol.* **176**, 5802–5813

45. Choder, M. (1991) A general topoisomerase I-dependent transcriptional repression in the stationary phase in yeast. *Genes Dev.* **5**, 2315–2326

46. Valcourt, J. R., Lemons, J. M. S., Haley, E. M., Kojima, M., Demuren, O. O., and Coller, H. A. (2012) Staying alive: metabolic adaptations to quiescence. *Cell Cycle* **11**, 1680–1696

47. Werner-Washburne, M., Braun, E. L., Crawford, M. E., and Peck, V. M. (1996) Stationary phase in Saccharomyces cerevisiae. *Mol. Microbiol.* **19**, 1159–1166

48. Paalme, T., Elken, R., Vilu, R., and Korhola, M. (1997) Growth efficiency of Saccharomyces cerevisiae on glucose/ethanol media with a smooth change in the dilution rate (A-stat). *Enzyme Microb. Technol.* **20**, 174–181

49. Özcan, S., and Johnston, M. (1999) Function and regulation of yeast hexose transporters. *Microbiol. Mol. Biol. Rev.* **63**, 554–569

50. Ozcan, S., and Johnston, M. (1995) Three different regulatory mechanisms enable yeast hexose transporter (HXT) genes to be induced by different levels of glucose. *Mol. Cell. Biol.* **15**, 1564–1572

51. Fraenkel, D. G. (2003) The top genes: on the distance from transcript to function in yeast glycolysis. *Curr. Opin. Microbiol.* **6**, 198–201

52. Thomson, J. M., Gaucher, E. A., Burgan, M. F., Kee, D. W. de, Li, T., Aris, J. P., *et al.* (2005) Resurrecting ancestral alcohol dehydrogenases from yeast. *Nat. Genet.* **37**, 630–635

53. Camarasa, C., Faucet, V., and Dequin, S. (2007) Role in anaerobiosis of the isoenzymes for Saccharomyces cerevisiae fumarate reductase encoded by OSM1 and FRDS1. *Yeast* **24**, 391–401

54. Påhlman, A. K., Granath, K., Ansell, R., Hohmann, S., and Adler, L. (2001) The yeast glycerol 3-Phosphatases Gpp1p and Gpp2p are required for glycerol biosynthesis and differentially involved in the cellular responses to osmotic, anaerobic, and oxidative stress. *J. Biol. Chem.* **276**, 3555–3563

55. van Dijken, J. P., and Scheffers, W. A. (1986) Redox balances in the metabolism of sugars by yeasts. *FEMS Microbiol. Lett.* **32**, 199–224

56. Herrero, E., Ros, J., Bellí, G., and Cabiscol, E. (2008) Redox control and oxidative stress in yeast cells. *Biochim. Biophys. Acta* **1780**, 1217–1235

57. Han, D., Williams, E., and Cadenas, E. (2001) Mitochondrial respiratory chain-dependent generation of superoxide anion and its release into the intermembrane space. *Biochem. J.* **353**, 411–416

58. Kwast, K. E., Burke, P. V., and Poyton, R. O. (1998) Oxygen sensing and the transcriptional regulation of oxygen-responsive genes in yeast. *J. Exp. Biol.* **201**, 1177–1195

59. Snoek, I., and Steensma, H. Y. (2007) Factors involved in anaerobic growth of Saccharomyces cerevisiae. *Yeast* **24**, 1–10

60. Zavrel, M., Hoot, S. J., and White, T. C. (2013) Comparison of sterol import under aerobic and anaerobic conditions in three fungal species, Candida albicans, Candida glabrata, and Saccharomyces cerevisiae. *Eukaryot. Cell* **12**, 725–738

61. Bisschops, M. M., Vos, T., Martínez-Moreno, R., Cortés, P. T., Pronk, J. T., and Daran-Lapujade, P. (2015) Oxygen availability strongly affects chronological lifespan and thermotolerance in batch cultures of Saccharomyces cerevisiae. *Microb. Cell* **2**, 429–444

62. Boender, L. G. M., Almering, M. J. H., Dijk, M., van Maris, A. J. A., de Winde, J. H., Pronk, J. T., *et al*. (2011) Extreme calorie restriction and energy source starvation in Saccharomyces cerevisiae represent distinct physiological states. *Biochim. Biophys. Acta* **1813**, 2133–2144

63. François, J., and Parrou, J. L. (2001) Reserve carbohydrates metabolism in the yeast Saccharomyces cerevisiae. *FEMS Microbiol. Rev.* **25**, 125–145

64. Wilson, K., and McLeod, B. J. (1976) The influence of conditions of growth on the endogenous metabolism of Saccharomyces cerevisiae: effect on protein, carbohydrate, sterol and fatty acid content and on viability. *Antonie Van Leeuwenhoek* **42**, 397–410

65. Daran-Lapujade, P., Rossell, S., van Gulik, W. M., Luttik, M. A. H., de Groot, M. J. L., Slijper, M., *et al*. (2007) The fluxes through glycolytic enzymes in Saccharomyces cerevisiae are predominantly regulated at posttranscriptional levels. *Proc. Natl. Acad. Sci. U. S. A.* **104**, 15753–15758

66. Bruckmann, A., Hensbergen, P. J., Balog, C. I. A., Deelder, A. M., Brandt, R., Snoek, I. S. I., *et al*. (2009) Proteome analysis of aerobically and anaerobically grown Saccharomyces cerevisiae cells. *J. Proteomics* **71**, 662–669

67. Picotti, P., Clément-Ziza, M., Lam, H., Campbell, D. S., Schmidt, A., Deutsch, E. W., *et al*. (2013) A complete mass-spectrometric map of the yeast proteome applied to quantitative trait analysis. *Nature* **494**, 266–270

68. Boender, L. G. M., De Hulster, E. A. F., Van Maris, A. J. A., Daran-Lapujade, P. A. S., and Pronk, J. T. (2009) Quantitative physiology of Saccharomyces cerevisiae at near-zero specific growth rates. *Appl. Environ. Microbiol.* **75**, 5607–5614

69. Vos, T., Hakkaart, X. D. V., de Hulster, E. A. F., Van Maris, A. J. A., Pronk, J. T., and Daran-Lapujade, P. (2016) Maintenance-energy requirements and robustness of Saccharomyces cerevisiae at aerobic near-zero specific growth rates. *Microb. Cell Fact.* **15**, 1–20

70. Herman, P. K. (2002) Stationary phase in yeast. *Curr. Opin. Microbiol.* **5**, 602–607

71. Malina, C., Di Bartolomeo, F., Kerkhoven, E. J., and Nielsen, J. (2021) Constraint-based modeling of yeast mitochondria reveals the dynamics of protein import and iron-sulfur cluster biogenesis. *iScience* **24**, 103294

72. Lu, H., Kerkhoven, E. J., and Nielsen, J. (2022) Multiscale models quantifying yeast physiology: towards a whole-cell model. *Trends Biotechnol.* **40**, 291–305

73. Elsemman, I. E., Prado, A. R., Grigaitis, P., Albornoz, M. G., Harman, V., Holman, S. W., *et al*. (2022) Whole-cell modeling in yeast predicts compartment-specific proteome constraints that drive metabolic strategies. *Nat. Commun.* **13**, 801

74. Kolkman, A., Daran-Lapujade, P., Fullaondo, A., Olsthoorn, M. M. A., Pronk, J. T., Slijper, M., *et al*. (2022) Proteome allocations change linearly with the specific growth rate of Saccharomyces cerevisiae under glucose limitation. *Nat. Commun.* **2**, 1–12

75. Regueira, A., Lema, J. M., and Mauricio-Iglesias, M. (2021) Microbial inefficient substrate use through the perspective of resource allocation models. *Curr. Opin. Biotechnol.* **67**, 130–140

76. Chen, Y., Li, F., Mao, J., Chen, Y., and Nielsen, J. (2021) Yeast optimizes metal utilization based on metabolic network and enzyme kinetics. *Proc. Natl. Acad. Sci. U. S. A.* **118**, e2020154118

77. Keng, T. (1992) HAP1 and ROX1 form a regulatory pathway in the repression of HEM13 transcription in Saccharomyces cerevisiae. *Mol. Cell. Biol.* **12**, 2616–2623

78. Amillet, J. M., Buisson, N., and Labbe-Bois, R. (1995) Positive and negative elements involved in the differential regulation by heme and oxygen of the HEM13 gene (coproporphyrinogen oxidase) in Saccharomyces cerevisiae. *Curr. Genet.* **28**, 503–511

79. Jordá, T., and Puig, S. (2020) Regulation of ergosterol biosynthesis in saccharomyces cerevisiae. *Genes (Basel).* **11**, 1–18

80. Rintala, E., Toivari, M., Pitkänen, J. P., Wiebe, M. G., Ruohonen, L., and Penttilä, M. (2009) Low oxygen levels as a trigger for enhancement of respiratory metabolism in Saccharomyces cerevisiae. *BMC Genomics* **10**, 461

81. Van Hoek, P., Van Dijken, J. P., and Pronk, J. T. (1998) Effect of specific growth rate on fermentative capacity of baker's yeast. *Appl. Environ. Microbiol.* **64**, 4226–4233

82. Delgado, M. L., O'Connor, J. E., Azorín, I., Renau-Piqueras, J., Gil, M. L., and Gozalbo, D. (2001) The glyceraldehyde-3-phosphate dehydrogenase polypeptides encoded by the Saccharomyces cerevisiae TDH1, TDH2 and TDH3 genes are also cell wall proteins. *Microbiology* **147**, 411–417

83. Lu, M., Ammar, D., Ives, H., Albrecht, F., and Gluck, S. L. (2007) Physical interaction between aldolase and vacuolar H+-ATPase is essential for the assembly and activity of the proton pump. *J. Biol. Chem.* **282**, 24495–24503

84. Chen, Y., and Nielsen, J. (2016) Flux control through protein phosphorylation in yeast. *FEMS Yeast Res.* **16**, 1–14

85. den Ridder, M., Daran-lapujade, P., and Pabst, M. (2020) Shot-gun proteomics: why thousands of unidentified signals matter. *FEMS Yeast Res.* **20**, foz088

86. Deutsch, E. W., Bandeira, N., Sharma, V., Perez-Riverol, Y., Carver, J. J., Kundu, D. J., *et al*. (2020) The proteomexchange consortium in 2020: enabling "big data" approaches in proteomics. *Nucleic Acids Res.* **48**, D1145–D1152

87. Perez-Riverol, Y., Bai, J., Bandla, C., García-Seisdedos, D., Hewapathirana, S., Kamatchinathan, S., *et al*. (2022) The PRIDE database resources in 2022: a hub for mass spectrometry-based proteomics evidences. *Nucleic Acids Res.* **50**, D543–D552